

Evidence for an orbital dependent Mott transition in the ladders of $(\text{La}, \text{Ca})_{\text{x}}\text{Sr}_{14-\text{x}}\text{Cu}_{24}\text{O}_{41}$ derived by electron energy-loss spectroscopy.

Friedrich Roth,¹ Alexandre Revcolevschi,² Bernd Büchner,³ Martin Knupfer,³ and Jörg Fink^{3,4,5}

¹*Institute of Experimental Physics, TU Bergakademie Freiberg,
Leipziger Straße 23, D-09599 Freiberg, Germany*

²*Laboratoire de Physico-Chimie de l'État Solide, Université Paris-Sud, 91405 Orsay, France*

³*IFW Dresden, P.O. Box 270116, D-01171 Dresden, Germany*

⁴*Max Planck Institute for Chemical Physics of Solids, D-01187 Dresden, Germany*

⁵*Institute for Solid-State and Material Physics, Technical University Dresden, D-01062 Dresden, Germany*

(Dated: January 3, 2022)

The knowledge of the charge carrier distribution among the different orbitals of Cu and O is a precondition for the understanding of the physical properties of various Cu-O frameworks. We employ electron energy-loss spectroscopy to elucidate the charge carrier plasmon dispersion in $(\text{La}, \text{Ca})_{\text{x}}\text{Sr}_{14-\text{x}}\text{Cu}_{24}\text{O}_{41}$ in dependency of x as well as temperature. We observe that the energy of the plasmon increases upon increasing Ca content, which signals an internal charge redistribution between the two Cu-O subsystems. Moreover, contrary to an uncorrelated model we come to the conclusion that the holes transferred to the Cu_2O_3 ladders are mainly located in the bonding and not in the anti-bonding band. This is caused by an orbital dependent Mott transition.

I. INTRODUCTION

Thirty-three years after the discovery of high-temperature superconductivity in cuprates, [1] there is still no generally accepted theory of the mechanism of this phenomenon. The reason for this is that we do not understand the normal state strongly correlated electronic structure of CuO_2 layers doped with holes. A starting model for the electronic structure of cuprates was the one-band Hubbard or $t - J$ model [2]. In this model, a hole in the divalent Cu and a hole in the surrounding square of four O ions form a singlet that describes the electronic structure in a one-band Hamiltonian. In this way, internal degrees of freedom in the Cu-O square are not taken into account. This model replaced the much more complicated three-band models [3] of these charge transfer insulators [4]. There is an ongoing debate whether the $t - J$ model describes the measured band dispersion and whether it is able to explain high- T_c superconductivity [5–7].

A way to test the general validity of the $t - J$ model is to look at compounds which contain Cu-O structures that are similar to the two-dimensional CuO_2 layers in high- T_c superconductors. In a recent study of T-CuO [8], where the C_4 rotational symmetry is broken, the authors came to the conclusion that there occur strong deviations from the Zhang-Rice singlet picture.

Another possibility to study the validity of the Zhang-Rice singlet picture is to investigate the electronic structure of cuprates with a reduced dimension, e.g., the quasi-one-dimensional compound $(\text{La}, \text{Y}, \text{Sr}, \text{Ca})_{14}\text{Cu}_{24}\text{O}_{41}$ [9]. These materials are composed of alternating stacks of edge-sharing CuO_2 chains and two-leg Cu_2O_3 ladders. These are separated by strings of Sr, Ca, and La atoms. The subsystems are arranged in layers, and the layers are oriented in the crystallographic a, c plane, while they are stacked in an al-

ternating manner along the perpendicular b axis [10, 11]. Electronically, $\text{Ca}_x\text{Sr}_{14-x}\text{Cu}_{24}\text{O}_{41}$ is inherently doped with six holes per formula unit. Despite this doping level, the parent compound $\text{Sr}_{14}\text{Cu}_{24}\text{O}_{41}$ shows semiconducting behavior. The substitution of Sr by Ca causes the materials to become conductive, and at a high substitution level ($x = 13.6$) even superconductivity under high pressure has been observed [12], which renders $\text{Ca}_{13.6}\text{Sr}_{0.4}\text{Cu}_{24}\text{O}_{41}$ the first superconducting copper oxide material with a non-square lattice. Furthermore, charge order has been reported and discussed for $\text{Ca}_x\text{Sr}_{14-x}\text{Cu}_{24}\text{O}_{41}$, indicating a competition between superconductivity and charge ordering in the ladder sub-system. As the substitution of Sr by Ca is isoelectronic, the electronic changes in the materials have been explained by the occurrence of chemical pressure and thereby induced (i) charge transfer from the chains to the ladders, and (ii) singlets on the rungs of the ladders [9]. The hole distribution in $\text{Ca}_x\text{Sr}_{14-x}\text{Cu}_{24}\text{O}_{41}$ as a function of x has been controversially discussed, the number of holes in the ladders scatters by almost 100% [13–22].

Moreover, there is a strong spread in the distribution of the holes on the two O atoms, two on the legs and one on the rung in the Cu_2O_3 units of the ladders. If one assumes an equal distribution of the holes in the square of O atoms surrounding the Cu sites, as in the $t - J$ model, one would expect the same number of holes in the rungs and in the legs. Most of the previous studies came to the conclusion that the holes are predominantly on the rungs [9]. On the other hand, a more recent study concluded that for the holes accommodated on the ladders, leg sites are preferred to rung sites [20].

The two-leg ladders are a representative example between one-dimensional electronic systems forming a Luttinger liquid and the two-dimensional Cu-O layers in high- T_c superconductors. DFT calculations came to the conclusion that the low energy physics of the ladders can

be described by two bands close to the Fermi level: a bonding and an anti-bonding band along the c direction [23, 24]. Part of these bands has been detected in ARPES studies [25]. For the interpretation of magnetic and interband charge excitations, it was necessary to take into account correlation effects which were treated in the $t - J$ approximation [26]. Certainly, it would be interesting to perform experiments on these systems to test whether one has to go beyond this approximation.

The influence of electronic correlations in this class of materials is profound. The interplay of spin and charge degrees of freedom in both subsystems exhibits a rich variety of exotic spin and charge arrangements. As a consequence, it makes both the chains as well as the ladders extremely sensitive to variations of external parameters, such as temperature, doping, and pressure. Therefore, the evolution of the electronic and magnetic structure upon Ca substitution is one of the key issues for the development of a microscopic understanding in such a complex system.

Electron energy-loss spectroscopy (EELS) is a useful tool for the investigation of materials at all levels of complexity in the electronic spectrum [27]. The EELS cross section is proportional to the loss function $\Im[-1/\epsilon(\omega, \mathbf{q})]$, where $\epsilon(\omega, \mathbf{q}) = \epsilon_1(\omega, \mathbf{q}) + i\epsilon_2(\omega, \mathbf{q})$ is the momentum and energy-dependent complex dielectric function. In this way, EELS probes the collective electronic excitations of a solid under investigation. Furthermore, it allows momentum dependent measurements of the loss function, i.e., the observation of non-vertical transitions within the band structure of a solid [28, 29].

II. EXPERIMENTAL

Single crystals of $R_x\text{Sr}_{14-x}\text{Cu}_{24}\text{O}_{41}$ (with $R = \text{La}$ and Ca) were grown by using the traveling solvent floating zone method [30]. For the EELS measurements, thin films (~ 100 nm) were cut perpendicular to the crystal b -axis from these single crystals using an ultramicrotome equipped with a diamond knife. The films were then put onto standard transmission electron microscopy grids and transferred into the spectrometer. The measurements as a function of Ca substitution were carried out at room temperature with a dedicated transmission electron energy-loss spectrometer [28, 29] employing a primary electron energy of 172 keV. The energy and momentum resolution was set to be $\Delta E = 80$ meV and $\Delta q = 0.035 \text{ \AA}^{-1}$, respectively. In addition, the spectrometer is equipped with a He-cryostat, which allows investigating the loss function down to a sample temperature of 20 K, which has been done for $\text{Ca}_{11.5}\text{Sr}_{2.5}\text{Cu}_{24}\text{O}_{41}$. Before measuring the loss-function, the thin films have been characterized by *in-situ* electron diffraction, in order to orient the crystallographic axis with respect to the transferred momentum [31].

III. EXPERIMENTAL RESULTS

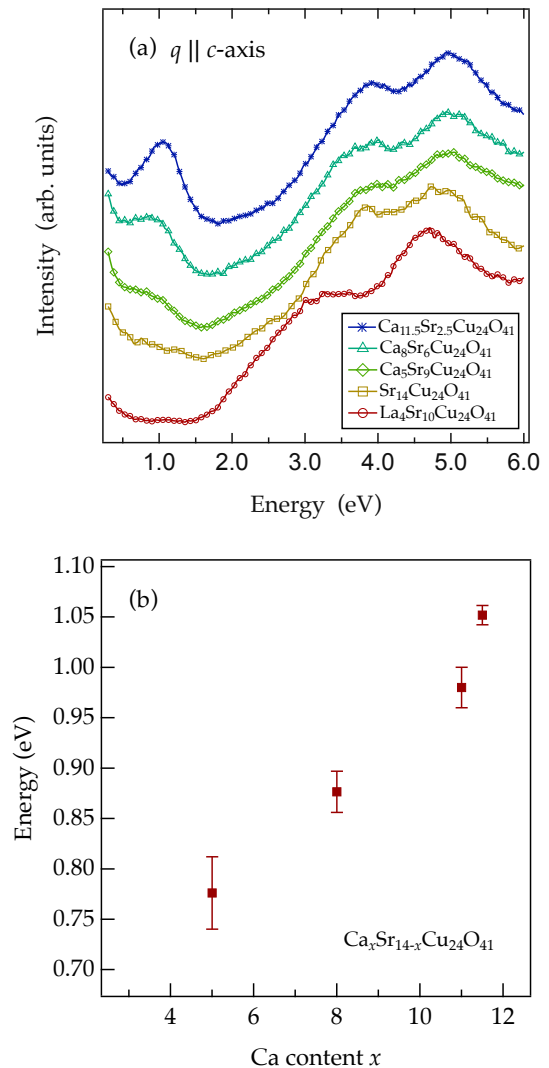


FIG. 1. (a) Loss functions for a small momentum transfer of 0.15 \AA^{-1} parallel to the c -axis for various $(\text{La}, \text{Y}, \text{Sr}, \text{Ca})_{14}\text{Cu}_{24}\text{O}_{41}$ compounds. The upturn near zero loss energy is due to the quasi-elastic line. (b) Energy position of the charge carrier plasmon as a function of the Ca concentration. The red squares represent the plasmon position evaluated from the measured spectra for $q = 0.15 \text{ \AA}^{-1}$.

We start the presentation of our results with the evolution of the loss function as a function of doping, for a momentum transfer of 0.15 \AA^{-1} parallel to the c -axis, as shown in Fig. 1 (a). In the energy range between 3 to 5 eV we see interband induced collective excitations which have been also detected in the edge-sharing CuO_2 chain compounds Li_2CuO_2 or CuGeO_3 [27, 32, 33]. According to our previous analysis, these excitations are localized excitations in the CuO_4 packet. They are localized because the hopping between the packets in these one-

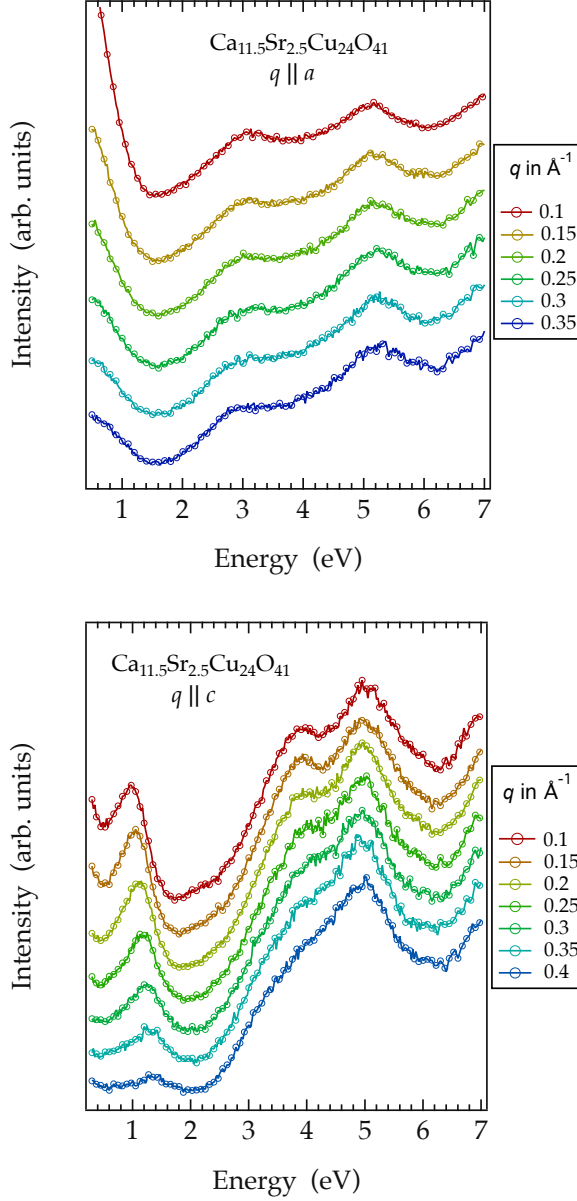


FIG. 2. Momentum dependence of the loss function of $\text{Ca}_{11.5}\text{Sr}_{2.5}\text{Cu}_{24}\text{O}_{41}$ for a momentum transfer q parallel to the crystallographic a (upper panel) and c (lower panel) axis. The data have been taken at 300 K.

dimensional edge-sharing Cu-O chains is small. Starting from the undoped compounds the energy of these excitations slightly increases with increasing doping concentration. These excitations are also detected for a momentum transfer parallel to the a -axis (see supplementary information and Ref. [31]). This observation supports the interpretation in terms of localized excitations.

In the energy range 2–3 eV there are dispersive excitations which according to our previous studies of the one dimensional corner sharing CuO_3 and CuO_2 chain compounds Sr_2CuO_3 and SrCuO_2 [27, 34], were ascribed to more delocalized charge transfer excitations [35–37], also

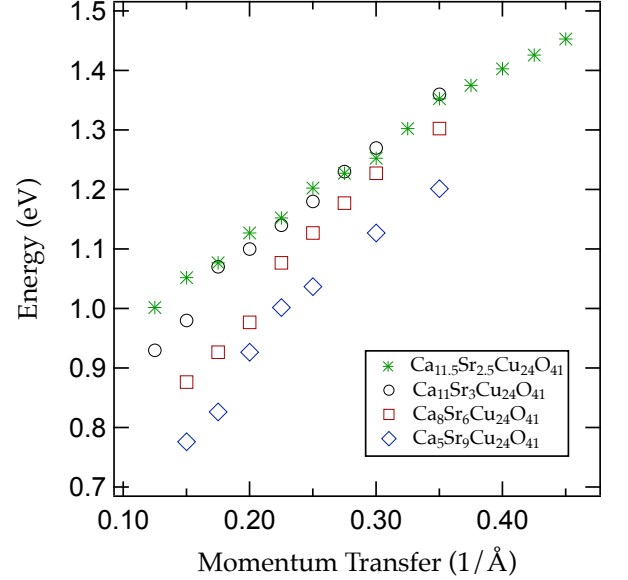


FIG. 3. Comparison of the plasmon dispersion in for various $(\text{Ca}, \text{Sr})_{14}\text{Cu}_{24}\text{O}_{41}$ compounds along the c direction at 300 K.

detected in 2D cuprates. These excitations are more pronounced for q parallel to the a -axis compared to q parallel to the c -axis (see supplementary information and Fig. 2).

Finally, a plasmon excitation is observed for $x \geq 0$ while for the undoped compound the plasmon is absent. Fig. 1 (b) depicts the respective plasmon energy with increasing Ca concentration. The observed plasmon energy is in very good agreement with previous data from reflectivity and EELS measurements (cf. Ref. [14, 31, 38]). Such a plasmon near 1 eV was also observed in the two-dimensional doped cuprates [39].

In Fig. 2 we present the loss function for momentum parallel to the a and c direction in $\text{Ca}_{11.5}\text{Sr}_{2.5}\text{Cu}_{24}\text{O}_{41}$ at room temperature. Clearly, the plasmon moves to higher energies upon increasing the momentum transfer. The higher energy features, in contrast, are almost independent of momentum. A plasmon dispersion has also been observed for other investigated $\text{Ca}_x\text{Sr}_{14-x}\text{Cu}_{24}\text{O}_{41}$ ($x = 5, 8, 11$) compounds, and we summarize these results in Fig. 3 and in the supplementary information. For q parallel a the charge transfer excitation near 3 eV is visible for all Ca concentrations.

Fig. 3 shows again the increasing plasmon energy at low momentum transfers with increasing Ca content in the ladder compounds (cf. Fig. 1 b)). Furthermore, it demonstrates that for all compositions we observe a finite plasmon intensity, dispersing to higher energies for a momentum transfer parallel to the c -axis (notice that for $x = 5, 8$ and 11 the plasmon peak is only detectable up to a momentum transfer of about 0.35 \AA^{-1} , which is caused by the strong damping as well as the low cross-section for higher momentum transfers). Fig. 3 reveals another intriguing observation. The slope of the plasmon dispersion also depends on the Ca substitution level. With

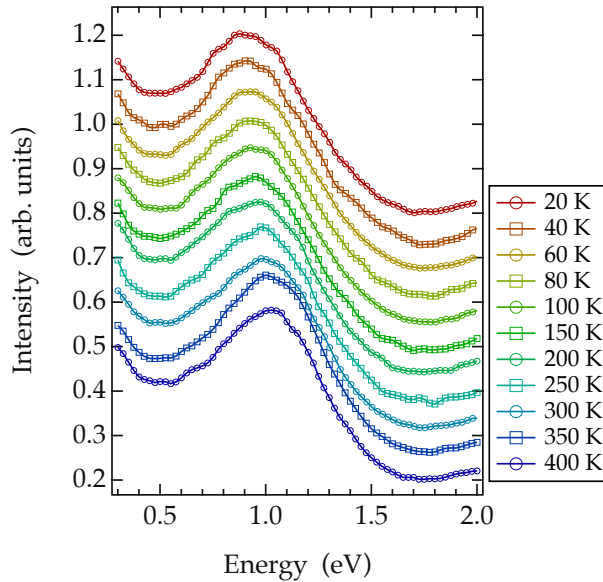


FIG. 4. Temperature dependence of the charge carrier plasmon in $\text{Ca}_{11.5}\text{Sr}_{2.5}\text{Cu}_{24}\text{O}_{41}$ for a momentum of 0.1 \AA^{-1} parallel to the c -axis.

increasing Ca content the slope of the dispersion curves is reduced.

Finally, we consider the temperature dependence of the plasmon energy in the compound $\text{Ca}_{11.5}\text{Sr}_{2.5}\text{Cu}_{24}\text{O}_{41}$. In Fig. 4 we show the temperature dependence of the plasmon feature in the loss function at a small momentum transfer of 0.1 \AA^{-1} measured at various temperatures in the range between 20 K and 400 K. As shown in Fig. 5, the plasmon energy clearly shifts to higher energies with increasing temperature. Moreover, the data indicate a somewhat stronger shift at lower temperatures (below about 150 K) as compared to the high-temperature region.

IV. CALCULATIONS

Experiments using optical spectroscopy and EELS, which are related to two-particle excitations, are normally much less sensitive to correlation effects than ARPES in which a single hole is excited. The reason for this is that dipoles are much less screened compared to a single hole. Nevertheless, in optical spectroscopy and EELS of cuprates clear differences in the spectra are observed between undoped and optimally doped compounds. In the former a Mott-Hubbard gap is observed while in the latter, due to a reduction of correlation effects, the gap is closed and a plasmon is detected [27, 40]. In this less correlated case the plasmon dispersion in optimally doped $\text{Bi}_2\text{Sr}_2\text{CaCu}_2\text{O}_8$ could be well described by RPA-type calculations [41]. Even the anisotropy of the band and the Fermi surface could be confirmed by this combination of EELS derived plasmon

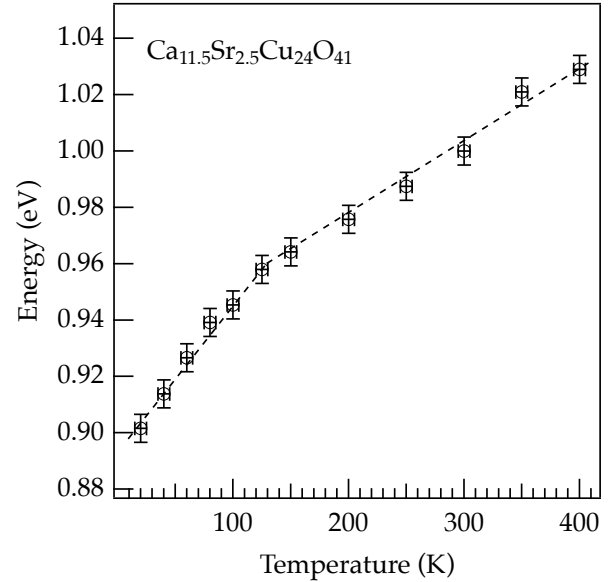


FIG. 5. Temperature dependent energy position of the charge carrier plasmon in $\text{Ca}_{11.5}\text{Sr}_{2.5}\text{Cu}_{24}\text{O}_{41}$ for a small momentum of 0.1 \AA^{-1} .

dispersions and those calculations. Therefore we started our RPA-type calculations of the plasmon dispersion in $\text{Ca}_x\text{Sr}_{14-x}\text{Cu}_{24}\text{O}_{41}$ on the basis of a tight-binding band structure for the weakly-doped ladders derived from the DFT approximation [23]. There are several experimental results that indicate that the edge-sharing chains have a gap larger than 2 eV and therefore do not contribute to the plasmon excitations in the energy range between 0.5 to 1.5 eV. In Fig. 6 we present the band structure for the Cu_2O_3 ladders calculated using the tight-binding parameters of the DFT calculations [23]. In this context, we point out that the band structure of the bonding band detected by ARPES [25] is very close to the DFT results.

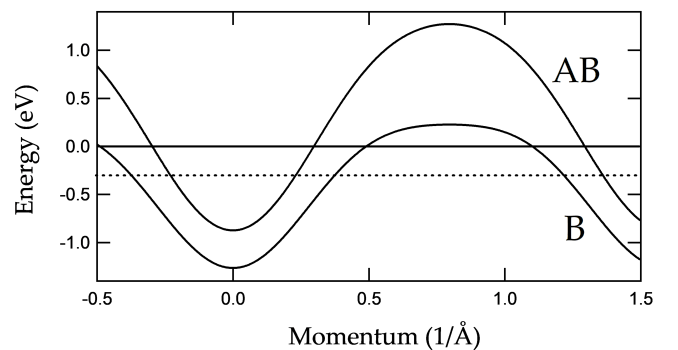


FIG. 6. Typical bonding (B) and antibonding (AB) band for the ladders in $\text{Ca}_x\text{Sr}_{14-x}\text{Cu}_{24}\text{O}_{41}$ along the c -axis used in the present calculations. The solid black horizontal line marks the Fermi level for an almost undoped (relative to divalent Cu) compound while the dashed line marks a Fermi level for a ladder which is about 20 % doped relative to divalent Cu.

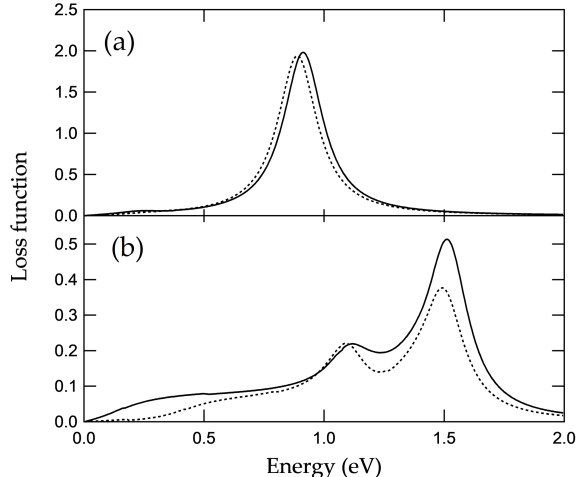


FIG. 7. Calculated energy dependence of the loss function $\Im(-1/\epsilon)$ for intra-band transitions in the anti-bonding and bonding band in $\text{Ca}_x\text{Sr}_{14-x}\text{Cu}_{24}\text{O}_{41}$. Solid line: undoped ladder ($x \approx 0$). Dashed line: doped ladder with a hole concentration of about 20 % corresponding to $x \approx 14$. (a) Momentum transfer $q=0.1 \text{ \AA}^{-1}$. (b) Momentum transfer $q=0.45 \text{ \AA}^{-1}$.

For the calculation of the complex dielectric function we used the Ehrenreich-Cohen expression [42]:

$$\epsilon(\omega, q) = \epsilon_\infty - \frac{A}{q^2} \int_{-\infty}^{\infty} \frac{\Delta F \Delta E}{\omega^2 - \Delta E^2 + i\Gamma\omega} dk. \quad (1)$$

Here $\Delta E = E_{k+q} - E_k$ and $\Delta F = F_{k+q} - F_k$ where F is the Fermi function. Using the complex dielectric function we then calculate the loss function $\Im[-1/\epsilon(\omega, q)]$. Calculating the maximum of the loss function for a particular momentum q as a function of energy yields the plasmon dispersion as a function of the momentum q . The effective mass for the band renormalization was adjusted to the experiment in such a way that the plasmon energy at the highest q values corresponds to the experimental data. The reason for this is that the plasmon energy at high q is essentially determined by the total bandwidth. Mass enhancements between 1.1 and 1.3 have been used for the calculations. On the other hand, the background dielectric function was adjusted in order to fit the plasmon energy at low momentum transfer, and it was kept constant thereafter.

In Fig.7 we present the calculated loss function for the sum of intra-band transitions in the bonding and anti-bonding band. Inter-band transitions are not allowed due to symmetry reasons. There are two maxima in the loss functions corresponding to plasmons related to intra-band transitions in the bonding and the anti-bonding band. At low momentum transfer, the plasmon of the bonding band is strongly over-damped due to the large real part of the dielectric function from the anti-

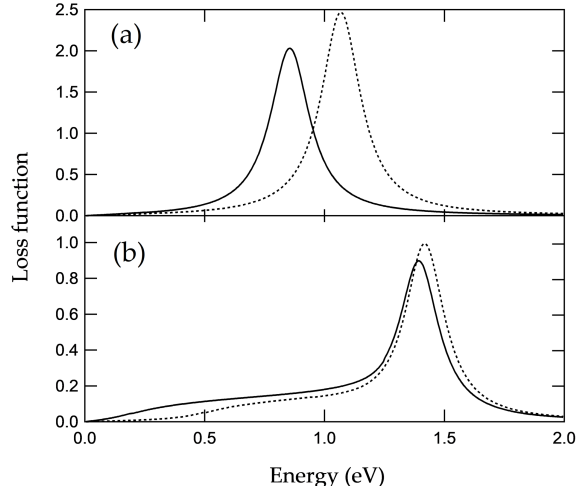


FIG. 8. Calculated energy dependence of the loss function $\Im(-1/\epsilon)$ for intra-band transitions in the bonding band in $\text{Ca}_x\text{Sr}_{14-x}\text{Cu}_{24}\text{O}_{41}$. Solid line: undoped ladder ($x \approx 0$). Dashed line: doped ladder with a hole concentration of about 20 % corresponding to $x \approx 14$. (a) Momentum transfer $q=0.1 \text{ \AA}^{-1}$. (b) Momentum transfer $q=0.45 \text{ \AA}^{-1}$.

bonding band in that energy range. At higher momentum transfer both plasmons are clearly visible. The fact that two plasmons are observed in the calculations but only one is detected in the EELS spectrum as well as almost no shifts are observed in the calculated spectrum while large shifts are observed upon doping at small momentum transfer indicates that the starting point in the calculation is wrong.

Much better agreement between experiment and calculations can be achieved when we assume that only the bonding band contributes to the measured spectral weight of the loss function. The results for this model are shown in Fig.8. Now we observe a larger shift of the plasmon energy at small momentum transfer $q=0.1 \text{ \AA}^{-1}$ upon replacement of Sr by Ca in agreement with the experimental results. At high momentum transfer, the shift is strongly reduced.

In Fig.9 we present the plasmon dispersion evaluated from the maximum of the plasmon. Again these results show a large shift of the plasmon energy upon Ca doping at low momentum transfer while at higher q the shift is reduced. The explanation of this result is that at low q the plasmon is determined by the Fermi velocity [39] which changes considerably upon doping. At higher q the plasmon energy is more determined by the bandwidth which does not change upon doping.

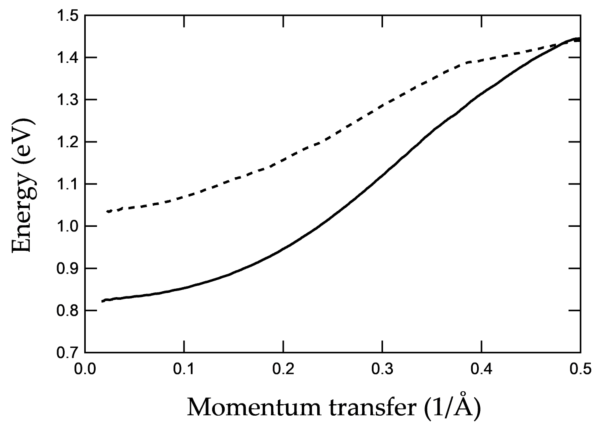


FIG. 9. Calculated plasmon dispersion (momentum dependence of the maximum of the loss function $\Im(-1/\epsilon)$) for intra-band transitions in the bonding band in $\text{Ca}_x\text{Sr}_{14-x}\text{Cu}_{24}\text{O}_{41}$. Solid line: undoped compound ($x \approx 0$). Dashed line: doped compound with a hole concentration of about 20 % corresponding to $x \approx 14$.

V. DISCUSSION

Firstly we discuss the higher energy excitations. Looking at the peaks near 5 eV, they show almost no dispersion for $q||a$ and c (see supplementary information), typical of a localized excitation in edge-shared CuO_2 chains, existing in Li_2CuO_2 or CuGeO_3 [27, 32, 33]. Also the peak near 3 eV shows almost no dispersion in agreement with previous EELS studies on edge-shared CuO_2 chains. Compared to the undoped corner-sharing quasi one-dimensional Sr_2CuO_3 [34] and the double chain SrCuO_2 [27], the charge transfer peak at 2-3 eV is shifted into the energy range 3-4 eV. This peak is also visible at 2.7 eV in the undoped 2D cuprates, e.g., in $\text{Sr}_2\text{CuO}_2\text{Cl}_2$ [27, 43]. The results of resonant inelastic x-ray scattering (RIXS) of $\text{Ca}_x\text{Sr}_{14-x}\text{Cu}_{24}\text{O}_{41}$ (Ref. [35–37]) are in good agreement with our assignment of the spectral structures in the energy range between 2-5 eV.

Next, we discuss the plasmon excitation which is the central point of the present study. Previous studies of $\text{Ca}_x\text{Sr}_{14-x}\text{Cu}_{24}\text{O}_{41}$ clearly indicated that upon Ca doping there is a transfer of holes from the chain to the ladders [14, 16–22]. This indicates that the plasmon is due to excitations in the ladders. The chains do not contribute to the plasmon excitation because the holes are still localized although the doping concentration is rather high. In the unsubstituted compound, the valency of Cu is near +2.6. The reason that the chains remain gaped and do not contribute to the plasmon excitation is that the hopping integral is probably much smaller than the onsite Coulomb interaction U . This view is in line with the weak reduction of the spectral weight in the upper Hubbard band upon doping [39]. Thus the plasmon excitation exclusively occurs in the ladders. Most of the previous studies indicate that the number of holes on the

ladders of $\text{Sr}_{14}\text{Cu}_{24}\text{O}_{41}$ is small and of the order of 1 per formula unit, corresponding to a Cu valency of +2.05. The increase of the plasmon energy with increasing Ca substitution [see Fig. 1 (b)] has also been discussed in a previous optical study [14].

Our data clearly signal that there is a visible temperature dependence of the hole number in the ladders in $\text{Ca}_{11.5}\text{Sr}_{2.5}\text{Cu}_{24}\text{O}_{41}$ (see Figs. 4 and 5). Evidence for such a hole reduction upon cooling had been reported previously from structural investigations and the related analysis of the bond-valence sum [17, 19]. The observed changes in bond lengths and angles together with the bond-valence sums have been interpreted in terms of a slight hole back-flow to the chains at low temperatures. This scenario is supported by the present EELS data. The small temperature-dependent change of the slope of the plasmon energy below 200 K (see Fig. 5) may be related to the proximity to a transition into charge density wave (CDW) state in which for smaller x the holes are ordered below $T_c = 250$ K [44–46]. Possibly the localization of the holes in the CDW state may cause a reduction of the plasmon energy. We emphasize that the opening of a small CDW gap of the order of 0.1 eV would only slightly increase the plasmon energy. On the other hand, a mass enhancement in the CDW state would decrease the plasmon energy and could thus explain the shift to lower energies at lower temperatures.

As described in Section IV the calculation of the loss function for a sum of uncorrelated bonding and anti-bonding band predicts that in this case the loss function is dominated by the plasmon of the anti-bonding band, because that of the bonding band is strongly damped. The energy of an intra-band plasmon at low momentum transfer is directly related to the Fermi velocity [41]. This Fermi velocity does almost not change for the anti-bonding band upon doping (see Fig. 6). Therefore, the difference in the energy between low and high Ca concentration would be expected to be small. Shifts of the plasmon related to the bonding band can hardly be detected because of the low intensity of that plasmon.

On the other hand, the calculation using the bonding band only leads to results that are close to the presented EELS data (see Figs. 3 and 9). In this case, the Fermi velocity strongly changes with increasing Ca concentration. For small doping, it is low because the Fermi level is close to the top of the bonding band. At higher hole doping the Fermi level moves to higher binding energies (see Fig. 6) and therefore the Fermi energy increases leading to a higher plasmon energy which is in agreement with the experimental EELS data. At higher momentum, the plasmon energy is determined by the full width of the conduction band which only slightly changes upon doping. This is again in agreement with the experiment. From these results we conclude that the nearly half-filled anti-bonding band remains gapped due to correlation effects and that the holes which are transferred from the chains to the ladders upon Ca substitution move into the bonding band. The correlation effects have a weaker

impact on the bonding band because it is only weakly doped. The conclusion that only the bonding band contributes to the plasmon excitation is also supported by the result, that at higher momentum only one plasmon is observed while in the case when both bands are active, the calculation predicts two plasmons (see Fig. 7). Finally, the result that a model which does not take into account correlation effects cannot describe the measured loss function is fostered by the consideration that in the uncorrelated case at a small hole concentration ($x = 0$) the half-filled anti-bonding band should be related to a strong plasmon excitation. In the experiment, however, for $x = 0$ the plasmon is hardly detectable [see Fig. 1 (a)].

The bonding band, having most of the charge density between the legs of the ladder, has probably mainly $2p$ character from the O ions on the rungs. On the other hand, the anti-bonding band has probably mainly O $2p$ character on the legs of the ladders on O $2p$ orbitals which could be parallel a or c . Our observation of holes on the O sites in the rungs supports the conception that hole doping of the symmetric bonding band leads to an anti-symmetric spin-singlet of the rungs. This means that the low energy charge density wave and superconductivity is based on singlets on the rungs. Our interpretation of the difference between bonding and anti-bonding band is supported by the observation that even for high Ca concentrations, the charge transfer excitation is detected for $q||a$ (see Fig. 2). This could be related to our postulation that the anti-bonding band is gapped by correlation effects and that the wave function of this anti-bonding band has strong contributions from O $2p$ orbitals parallel to the a -axis. We emphasize that from the present work, we only obtain information on the hole distribution between bonding and anti-bonding band. However, we do not obtain any information on the hole distribution on the four O $2p$ orbitals along the a and the c -axis on the rungs and the legs. Possibly calculations beyond the $t - J$ model together with our experimental EELS results could provide more detailed information.

Our interpretation of the plasmon dispersion in these compounds in terms of doping of the rungs is supported by various other experimental results. The XAS results on $\text{Ca}_x\text{Sr}_{14-x}\text{Cu}_{24}\text{O}_{41}$ indicate that upon replacement of Sr by Ca, the holes move into O $2p$ orbitals on the rungs while the hole number on O $2p$ orbitals parallel to the legs remain constant [16].

In the following, we compare our EELS results with ARPES data of $\text{Ca}_x\text{Sr}_{14-x}\text{Cu}_{24}\text{O}_{41}$ published in the literature. For the compound without Ca ($x = 0$) Koitzsch et al. [25] have detected a bonding and an antibonding band, the dispersions of which are close to that derived from DFT calculations [23]. It is interesting to note that spectral weight below a binding energy of 0.4 eV is only detected for the bonding band but not for the anti-bonding. This could be interpreted as a formation of a correlation induced gap for the anti-bonding band but not for the less correlated bonding band. This ARPES result would support our interpretation of the EELS

data. On the other hand, for the Ca substituted compound ($x = 11.5$), Koitzsch et al. have detected no bonding band, but an anti-bonding band with a clear spectral weight close to the Fermi level. This result would be at variance with our interpretation of the plasmon dispersion which needs a gapped anti-bonding band to explain the absence of a second plasmon. However, in another ARPES study by Yoshida et al. [47] it was emphasized that there is a clear absence of a quasiparticle peak at the Fermi level in the ARPES data of $\text{Ca}_x\text{Sr}_{14-x}\text{Cu}_{24}\text{O}_{41}$ which is completely different from ARPES spectra of optimally doped high- T_c superconductors with a half-filled band [48, 49]. The authors came to the conclusion that there is a gap caused by a charge density wave. Finally, a study by Takahashi et al [50] on the unsubstituted compound ($x = 0$) detected a gap of 0.4 eV which was assigned to a Mott-Hubbard gap. This would support our analysis of the plasmon dispersion. A further ARPES study by Sato et al. [51] detected a similar spectral weight even in the substituted sample ($x = 11.5$) indicating a correlation induced gap even in the substituted compound. These findings are in line with the results derived from the analysis of the present plasmon dispersion. Summarizing the comparison presented in this paragraph yields in some cases a support of our EELS analysis by ARPES, in other cases, there exists no agreement. Moreover, we want to emphasize that EELS, in contrast to APRES, is a more bulk-sensitive method—independent from the surface conditions as well as cleanness of the sample. Therefore, the presented results help to get a deeper insight into the microscopic electronic structure of that complex system and can be used to finally clear up the published conflicting ARPES results as discussed above.

The cuprate ladder compounds are in some way the intermediate systems between the doped 1D systems forming a Luttinger liquid with spinon and holons and the two-dimensional cuprates, which in the overdoped case form a Fermi liquid. The $t - J$ model [2] is believed to represent the gross features of the electronic structure of the two-dimensional cuprates. In this model, the charge carriers can be described by singlet particles formed by a Cu $3d$ hole on the divalent Cu site and a O $2p$ hole on the surrounding O square. In theoretical studies, it also was tried to describe the charge carriers in a two-leg ladder by a $t - J$ model [26, 52]. The charge excitations in the Cu-O ladders cannot be described by a one-particle Hamiltonian based on Zhang-Rice singlets. Rather the results point to an orbital dependent Mott transition for the two-leg layer, leading to the formation of mobile singlet holes on the rungs, related to the bonding band and in the anti-bonding band a Mott-Hubbard state, or more precise a charge transfer insulator. Our results thus may question also the application of the Zhang-Rice singlet model for the precise description of the electronic structure of the two-dimensional cuprate high- T_c superconductors.

VI. SUMMARY

We have investigated the charge carrier plasmon in the spin-ladder compound $\text{Ca}_x\text{Sr}_{14-x}\text{Cu}_{24}\text{O}_{41}$ as a function of Ca substitution and temperature using electron energy-loss spectroscopy. The energy of the plasmon increases upon increasing Ca content, which signals an increasing number of holes in the Cu_2O_3 ladders due to an internal charge redistribution between chains and ladders. A comparison of the experimental plasmon excitations with RPA-like calculations for the bonding and anti-bonding band indicates that the holes, which are transferred from the chain and the ladder upon replacement of Sr by Ca, are mainly located in the rungs. The reason for this is the different filling of the bonding and antibonding band leading to a Mott Hubbard splitting for the half-filled anti-bonding band and rather

mobile charge carriers in the bonding band having predominantly O $2p$ character with orbitals along the rungs. Thus the charge carriers cannot be described by Zhang-Rice singlets very often employed for the 2D cuprates. Rather in the ladder system which is between the 1D and the 2D cuprates, the charge carriers are singlets on the rungs fundamentally different from those of the 1D and 2D cuprates. Our results may question the general application of the $t - J$ model to cuprate high- T_c superconductors.

ACKNOWLEDGMENTS

We thank M. Naumann, R. Hübel, F. Thunig and S. Leger for technical assistance. We acknowledge fruitful discussions with C. Wohlleben, J. Lorenzano, and R. Eder.

-
- [1] J. Bednorz and K. Müller, *Z. Phys. B* **64**, 189 (1986).
 - [2] F. C. Zhang and T. M. Rice, *Phys. Rev. B* **37**, 3759 (1988).
 - [3] V. J. Emery, *Phys. Rev. Lett.* **58**, 2794 (1987).
 - [4] J. Zaanen, G. A. Sawatzky, and J. W. Allen, *Phys. Rev. Lett.* **55**, 418 (1985).
 - [5] B. Lau, M. Berciu, and G. A. Sawatzky, *Phys. Rev. Lett.* **106**, 036401 (2011).
 - [6] H. Ebrahimnejad, G. A. Sawatzky, and M. Berciu, *Nat. Physics* **10**, 951 (2014).
 - [7] H. Ebrahimnejad, G. A. Sawatzky, and M. Berciu, *J. of Physics: Condensed Matter* **28**, 105603 (2016).
 - [8] C. P. J. Adolphs, S. Moser, G. A. Sawatzky, and M. Berciu, *Phys. Rev. Lett.* **116**, 087002 (2016).
 - [9] T. Vuletić, B. Korin-Hamzić, T. Ivek, S. Tomić, B. Gorshunov, M. Dressel, and J. Akimitsu, *Physics Reports* **428**, 169 (2006).
 - [10] E. McCarron, M. Subramanian, J. Calabrese, and R. Harlow, *Mater. Res. Bull.* **23**, 1355 (1988).
 - [11] T. Siegrist, L. Schneemeyer, S. Sunshine, J. Waszczak, and R. Roth, *Mater. Res. Bull.* **23**, 1429 (1988).
 - [12] M. Uehara, T. Nagata, J. Akimitsu, H. Takahashi, N. Mori, and K. Kinoshita, *J. Phys. Soc. Jpn.* **65**, 2764 (1996).
 - [13] M. Kato, K. Shiotani, and Y. Koike, *Physica C: Superconductivity* **258**, 284 (1996).
 - [14] T. Osafune, N. Motoyama, H. Eisaki, and S. Uchida, *Phys. Rev. Lett.* **78**, 1980 (1997).
 - [15] K. Magishi, S. Matsumoto, Y. Kitaoka, K. Ishida, K. Asayama, M. Uehara, T. Nagata, and J. Akimitsu, *Phys. Rev. B* **57**, 11533 (1998).
 - [16] N. Nücker, M. Merz, C. A. Kuntscher, S. Gerhold, S. Schuppler, R. Neudert, M. S. Golden, J. Fink, D. Schild, S. Stadler, V. Chakarian, J. Freeland, Y. U. Idzerda, K. Conder, M. Uehara, T. Nagata, J. Goto, J. Akimitsu, N. Motoyama, H. Eisaki, S. Uchida, U. Ammerahl, and A. Revcolevschi, *Phys. Rev. B* **62**, 14384 (2000).
 - [17] M. Isobe, M. Onoda, T. Ohta, F. Izumi, K. Kimoto, E. Takayama-Muromachi, A. Hewat, and K. Ohoyama, *Phys. Rev. B* **62**, 11667 (2000).
 - [18] A. Rusydi, M. Berciu, P. Abbamonte, S. Smadici, H. Eisaki, Y. Fujimaki, S. Uchida, M. Rübhausen, and G. A. Sawatzky, *Phys. Rev. B* **75**, 104510 (2007).
 - [19] G. Deng, V. Pomjakushin, V. Petříček, E. Pomjakushina, M. Kenzelmann, and K. Conder, *Phys. Rev. B* **84**, 144111 (2011).
 - [20] V. Ilakovac, C. Gougoussis, M. Calandra, N. Brookes, V. Bisogni, S. Chiuzaian, J. Akimitsu, O. Milat, S. Tomić, and C. Hague, *Phys. Rev. B* **85**, 075108 (2012).
 - [21] M.-J. Huang, G. Deng, Y. Chin, Z. Hu, J.-G. Cheng, F. Chou, K. Conder, J.-S. Zhou, T.-W. Pi, J. Goodenough, *et al.*, *Phys. Rev. B* **88**, 014520 (2013).
 - [22] M. Bugnet, S. Löffler, D. Hawthorn, H. A. Dabkowska, G. M. Luke, P. Schattschneider, G. A. Sawatzky, G. Radtke, and G. A. Botton, *Sci. Adv.* **2**, e1501652 (2016).
 - [23] M. Arai and H. Tsunetsugu, *Phys. Rev. B* **56**, R4305 (1997).
 - [24] T. F. A. Müller, V. Anisimov, T. M. Rice, I. Dasgupta, and T. Saha-Dasgupta, *Phys. Rev. B* **57**, R12655 (1998).
 - [25] A. Koitzsch, D. S. Inosov, H. Shiozawa, V. B. Zabolotnyy, S. V. Borisenko, A. Varykhalov, C. Hess, M. Knupfer, U. Ammerahl, A. Revcolevschi, and B. Büchner, *Phys. Rev. B* **81**, 113110 (2010).
 - [26] U. Kumar, A. Nocera, E. Dagotto, and S. Johnston, *Phys. Rev. B* **99**, 205130 (2019).
 - [27] J. Fink, M. Knupfer, S. Atzkern, and M. Golden, *J. Electron Spectrosc. Relat. Phenom.* **117**, 287 (2001).
 - [28] J. Fink, *Adv. Electron. Electron Phys.* **75**, 121 (1989).
 - [29] F. Roth, A. König, J. Fink, B. Büchner, and M. Knupfer, *J. Electron. Spectrosc. Relat. Phenom.* **195**, 85 (2014).
 - [30] U. Ammerahl, G. Dhalenne, A. Revcolevschi, J. Berthon, and H. Moudden, *J. Cryst. Growth* **193**, 55 (1998).
 - [31] F. Roth, C. Hess, B. Büchner, U. Ammerahl, A. Revcolevschi, and M. Knupfer, *Phys. Rev. B* **82**, 245110 (2010).

- [32] S. Atzkern, M. Knupfer, M. S. Golden, J. Fink, C. Waidacher, J. Richter, K. W. Becker, N. Motoyama, H. Eisaki, and S. Uchida, *Phys. Rev. B* **62**, 7845 (2000).
- [33] S. Atzkern, M. Knupfer, M. S. Golden, J. Fink, A. Hübsch, C. Waidacher, K. W. Becker, W. v. d. Linden, M. Weiden, and C. Geibel, *Phys. Rev. B* **64**, 075112 (2001).
- [34] R. Neudert, M. Knupfer, M. Golden, J. Fink, W. Stephan, K. Penc, N. Motoyama, H. Eisaki, and S. Uchida, *Phys. Rev. Lett.* **81**, 657 (1998).
- [35] L. Wray, D. Qian, D. Hsieh, Y. Xia, T. Gog, D. Casa, H. Eisaki, and M. Hasan, *Physica B* **403**, 1456 (2008).
- [36] L. Wray, D. Qian, D. Hsieh, Y. Xia, T. Gog, D. Casa, H. Eisaki, and M. Z. Hasan, *J. Phys. Chem. Solids* **69**, 3146 (2008).
- [37] K. Ishii, K. Tsutsui, T. Tohyama, T. Inami, J. Mizuki, Y. Murakami, Y. Endoh, S. Maekawa, K. Kudo, Y. Koike, and K. Kumagai, *Phys. Rev. B* **76**, 045124 (2007).
- [38] B. Ruzicka, L. Degiorgi, U. Ammerahl, G. Dhalenne, and A. Revcolevschi, *Eur. Phys. J. B* **6**, 301 (1998).
- [39] N. Nücker, H. Romberg, S. Nakai, B. Scheerer, J. Fink, Y. F. Yan, and Z. X. Zhao, *Phys. Rev. B* **39**, 12379 (1989).
- [40] S. Uchida, T. Ido, H. Takagi, T. Arima, Y. Tokura, and S. Tajima, *Phys. Rev. B* **43**, 7942 (1991).
- [41] N. Nücker, U. Eckern, J. Fink, and P. Müller, *Phys. Rev. B* **44**, 7155 (1991).
- [42] H. Ehrenreich and M. H. Cohen, *Phys. Rev.* **115**, 786 (1959).
- [43] J. Fink, R. Neudert, H. C. Schmelz, T. Böske, O. Knauff, S. Haffner, M. Knupfer, M. S. Golden, G. Krabbes, H. Eisaki, and S. Uchida, *Physica B: Condensed Matter* **237-238**, 93 (1997).
- [44] G. Blumberg, P. Littlewood, A. Gozar, B. S. Dennis, N. Motoyama, H. Eisaki, and S. Uchida, *Science* **297**, 584 (2002).
- [45] T. Vuletić, B. Korin-Hamzić, S. Tomić, B. Gorshunov, P. Haas, T. Röm, M. Dressel, J. Akimitsu, T. Sasaki, and T. Nagata, *Phys. Rev. Lett.* **90**, 257002 (2003).
- [46] P. Abbamonte, G. Blumberg, A. Rusydi, A. Gozar, P. G. Evans, T. Siegrist, L. Venema, H. Eisaki, E. D. Isaacs, and G. A. Sawatzky, *Nature* **431**, 1078 (2004).
- [47] T. Yoshida, X. J. Zhou, Z. Hussain, Z.-X. Shen, A. Fujimori, H. Eisaki, and S. Uchida, *Phys. Rev. B* **80**, 052504 (2009).
- [48] T. K. Kim, A. A. Kordyuk, S. V. Borisenko, A. Koitzsch, M. Knupfer, H. Berger, and J. Fink, *Phys. Rev. Lett.* **91**, 167002 (2003).
- [49] A. Koitzsch, S. V. Borisenko, A. A. Kordyuk, T. K. Kim, M. Knupfer, J. Fink, H. Berger, and R. Follath, *Phys. Rev. B* **69**, 140507 (2004).
- [50] T. Takahashi, T. Yokoya, A. Ashihara, O. Akaki, H. Fujisawa, A. Chainani, M. Uehara, T. Nagata, J. Akimitsu, and H. Tsunetsugu, *Phys. Rev. B* **56**, 7870 (1997).
- [51] T. Sato, T. Yokoya, T. Takahashi, M. Uehara, T. Nagata, J. Goto, and J. Akimitsu, *J. Phys. Chem. Solids* **59**, 1912 (1998).
- [52] E. Dagotto and T. M. Rice, *Science* **271**, 618 (1996).